Bioactive Materials 5 (2020) 644–658

Contents lists available at ScienceDirect

Bioactive Materials

journal homepage: http://www.keaipublishing.com/biomat

Insitu magnesium calcium phosphate cements formation: From one pot powders precursors synthesis to *in vitro* investigations

M.A. Goldberg[a,*], P.A. Krohicheva[a], A.S. Fomin[a], D.R. Khairutdinova[a], O.S. Antonova[a], A.S. Baikin[a], V.V. Smirnov[a], A.A. Fomina[a], A.V. Leonov[b], I.V. Mikheev[b], N.S. Sergeeva[c], S.A. Akhmedova[c], S.M. Barinov[a], V.S. Komlev[a]

[a] A.A. Baikov Institute of Metallurgy and Materials Science, Russian Academy of Sciences, 119334, Leninsky av, 49, Moscow, Russian Federation
[b] M.V. Lomonosov Moscow State University, Department of Chemistry, 119991, Leninskie Gory, 1, Moscow, Russian Federation
[c] Federal State Budgetary Institution National Medical Research Radiological Center of the Ministry of Health of the Russian Federation, 125284, 2nd Botkinsky pass., 3, Moscow, Russian Federation

ARTICLE INFO

Keywords:
Magnesium calcium phosphate cement
Stanfieldite
Whitlockite
Newberyite
Brushite
In vitro investigations

ABSTRACT

Calcium phosphate cements are of great interest for researchers and their applications in medical practice expanded. Nevertheless, they have a number of drawbacks including the insufficient level of mechanical properties and low degradation rate. Struvite ($MgNH_4PO_4$) -based cements, which grew in popularity in recent years, despite their neutral pH and acceptable mechanical performance, release undesirable NH_4^+ ions during their resorption. This issue could be avoided by replacement of ammonia ions in the cement liquid with sodium, however, such cements have a pH values of 9–10, leading to cytotoxicity.

Thus, the main goal of this investigation is to optimize the composition of cements to achieve the combination of desirable properties: neutral pH, sufficient mechanical properties, and the absence of cytotoxicity, applying Na_2HPO_4-based cement liquid. For this purpose, cement powders precursors in the $CaO–MgO–P_2O_5$ system were synthesized by one-pot process in a wide composition range, and their properties were investigated.

The optimal performance was observed for the cements with (Ca + Mg)/P ratio of 1.67, which are characterized by newberyite phase formation during setting reaction, pH values close to 7, sufficient compressive strength up to 22 ± 3 MPa (for 20 mol.% of Mg), dense microstructure and adequate matrix properties of the surface. This set of features make those materials promising candidates for medical applications.

1. Introduction

Injuries, surgical interventions in oncology, traumatology and orthopedics often lead to extensive bone defects. Ceramics made of calcium phosphates has been used in medicine for several decades [1–3] for bone restoration. However, they have several disadvantages: their application is mainly limited by low rate of bioresorption compared to the rate of formation of new bone tissue and the inability to fill defects of complex shape [2,3]. Calcium phosphate cements (CPCs) are free from the disadvantages inherent to ceramic materials, they are easy to use by therapists during surgery treatment, they can fill the defect space of any configuration, they are osteoconductive materials, i.e. able to support bone cell growth [1]. An important positive property of CPCs is the absence of exothermic effects, leading to burns and necrosis of surrounding tissues, which occurs when using polymeric acrylate-based polymer cements [4]. Cements based on $CaHPO_4*2H_2O$ are called brushite CPCs and have one undeniable advantage over other synthetic biomaterials intended for reconstruction of bone defects: the rate of their bioresorption is comparable to the rate of formation of new bone tissue [1]. Major concerns about a broad clinical use of brushite cements are their relatively poor mechanical properties compared to unresorbable apatite cements and their strong acidic pH value during setting which can lead to the release of acid into the surrounding tissue around the implant [5].

Peer review under responsibility of KeAi Communications Co., Ltd.
* Corresponding author.
E-mail addresses: mgoldberg@imet.ac.ru (M.A. Goldberg), polinariakroh@gmail.com (P.A. Krohicheva), afomin@imet.ac.ru (A.S. Fomin), dkhayrutdinova@imet.ac.ru (D.R. Khairutdinova), oantonova@imet.ac.ru (O.S. Antonova), baikinas@mail.ru (A.S. Baikin), smirnov2007@mail.ru (V.V. Smirnov), afomina@imet.ac.ru (A.A. Fomina), avleonov49@gmail.com (A.V. Leonov), mikheev.ivan@gmail.com (I.V. Mikheev), prognoz.06@mail.ru (N.S. Sergeeva), prognoz.06@mail.ru (S.A. Akhmedova), barinov_s@mail.ru (S.M. Barinov), komlev@mail.ru (V.S. Komlev).

https://doi.org/10.1016/j.bioactmat.2020.03.011
Received 30 November 2019; Received in revised form 17 March 2020; Accepted 22 March 2020

At the same time, over the past few years, magnesium phosphate bone cements (MPCs) have come to be seen as an alternative to CPCs. MPCs are obtained by reacting powdered magnesium oxide or magnesium phosphate with an acidic phosphate solution, which takes place with the dissolution of magnesium oxide and the subsequent formation of a cation solution with water. The dissolved cation of magnesium oxide or phosphate reacts with the phosphate anion to form an amorphous gel [6]. This gel crystallizes around unreacted particles of magnesium oxide or phosphate, forming a core-shell scheme with the formation of durable material [7]. The main compounds on the basis of which cement liquid containing a phosphate anion are phosphoric acid (H_3PO_4), monoammonium phosphate ($NH_4H_2PO_4$), disodium phosphate (Na_2HPO_4), and dipotassium phosphate (K_2HPO_4) [6]. The main disadvantages of MPCs based on MgO are an exothermic reaction that occurs during the setting and hardening of cement [8], which can lead to tissue necrosis. Also, magnesia-based cements are characterized by a high pH level in the range of 9–10, which can also lead to a toxic reaction when used in orthopedics [8,9]. To reduce the pH level of bone cement, the monoammonium phosphate cement liquid is applied with formation of magnesium phosphate mineral struvite ($MgNH_4PO_4$*$6H_2O$). Few studies have investigated struvite forming cements for biomedical applications and showed high strength of the materials (compressive strength up to 50 MPa) and an appropriate setting time of 3–10 min, which meets clinical demands [10]. However, the presence of NH_4^+ cation in the bone cements could led to undesirable release of ammonia in human body. On the one hand, such MPCs have high mechanical strength, on the other hand fast setting reaction limits the processing time by a surgeon [11]. To reduce the thermal effect and decrease the pH of cement materials, composite cements are developed, for example based on calcium silicate [12,13] or calcium sulfate [14].

The development of cements containing both magnesium and calcium phosphates (MCPCs) resulted in materials that combine the advantages of both components: high strength due to magnesium phosphate, lack of cytotoxicity, and enhanced matrix surface properties due to the presence of calcium phosphates [15]. There are various combinations of composite MCPCs used in the form of mechanical mixtures of powders taken in predetermined ratios, which make it possible to obtain both composite and single-phase cement materials [6]. As the magnesium components $Mg_3(PO_4)_2$ and MgO are used. The highest strength was achieved when tetracalcium phosphate (TeTCP) cement, dicalcium phosphate dihydrate, magnesium oxide and monoammonium phosphate were used as the powder phase of the cement and distilled water was used as the mixing liquid. These cements had a strength of up to 91 MPa, characterized by a setting time of about 6 min, and showed the absence of cytotoxicity *in vitro*, as well as improved osseointegration into the rabbit bone defect zone, as compared to CPCs without magnesium oxide [16]. High mechanical properties – compressive strength up to 43 MPa, accelerated weight loss when dissolved in fluids simulating extracellular fluids of the body and the absence of a toxic reaction were demonstrated by cements based on a mixture of magnesium oxide and calcium dihydrogen phosphate [17]. The disadvantage of mechanical mixtures of powder components when used as cement powder is the complexity in achieving the homogeneous distribution of the components in the mixture and the difference in their dissolution rate in the cement liquid. Previous studies on the struvite forming cements used multi-component mixtures of secondary ($MgHPO_4$) and tertiary ($Mg_3(PO_4)_2$) magnesium phosphates together with calcium orthophosphates (α-tricalcium phosphate (α-TCP), β-tricalcium phosphate (β-TCP), hydroxyapatite (HA)) as fillers [18]. Also, there are the powder cement system with the pre-introduced additional source of PO_4^{3-} in the form of Na_2HPO_4, $NH_4H_2PO_4$, K_2HPO_4. In the same time, MgO–P_2O_5 system does not have the compounds with Mg/P ratio of 1.67 or 2.0 as in the case of CaO–P_2O_5: HA and TeTCP. The increase of Mg/P ratio to values exceeding 1.5 resulted in the formation of farringtonite ($Mg_3(PO_4)_2$) mixture with MgO which could be applied as cement powders. The one-pot synthesis of cements powders precursors for MCPCs could be realized by formation of calcium-magnesium phosphate phase and highly active MgO phase during the precipitation in the media with an excess of Mg cations. The one-pot synthesis could be a simple route to reduce the problems associated with the manufacturing and handling of mechanical mixtures, including different particle sizes, difficult preparation of homogenous powder mixtures, de-mixing during transport or storage. The present work aimed at the fabrication of cement powders precursors by one-pot synthesis and investigation of the effect of different (Ca + Mg)/P ratio and Mg amount on the formation of materials in the whitlockite $Ca_xMg_{(3-x)}(PO_4)_2$, stanfieldite $Mg_3Ca_3(PO_4)_4$ and MgO system in the excess of cations. The cement liquid of NaH_2PO_4–Na_2HPO_4 is characterized by the absence NH_4^+ cations and optimal pH value in the 4.0–4.5 could be applied for cement paste and set cements obtaining [11]. The properties and behavior *in vitro* were investigated and optimal composition with neutral pH value of cement extract, acceptable mechanical properties and absence of cytotoxicity were developed.

2. Materials and methods

2.1. Cement powders synthesis and characterization

As a model of one-pot-synthesis of cement powders precursors we suggested aqueous precipitation method based on the mixing of $Mg(NO_3)_2$, $Ca(NO_3)_2$, $(NH_4)_2HPO_4$ and deionized water described in Ref. [15]. Powder synthesis was carried out according to reaction schemes 1–3 using reactants of an analytical grade (LTD Labtech, Russia) and deionized water. We did not expect the formation of Mg-substituted HA or TeTCP and assumed the formation of materials in the $Ca_{(3-x)}Mg_x(PO_4)_2$ and MgO system in the case of excess of cations, but used the listed theoretical reaction schemes based on calcium phosphate diagram [19] to calculate the amount of reactants:

$$(3-3x)Ca(NO_3)_2 + 3xMg(NO_3)_2 + 2NH_4OH + 2(NH4)_2HPO_4 = Ca_{(3-3x)}Mg_{3x}(PO_4)_2 + 6NH_4NO_3 + 2H_2O \quad (1)$$

$$(10-10x)Ca(NO_3)_2 + 10xMg(NO_3)_2 + 8NH_4OH + 6(NH_4)_2HPO_4 = Ca_{(10-10x)}Mg_{10x}(PO_4)_6(OH)_2 + 20NH_4NO_3 + 6H_2O \quad (2)$$

$$4(1-x)Ca(NO_3)_2{\cdot}+{\cdot}4xMg(NO_3)_2{\cdot}+{\cdot}4(NH_4)_2HPO_4{\cdot}+{\cdot}8NH{\cdot}OH{\cdot}= {\cdot}Ca_{(4-4x)}{\cdot}Mg_{4x}O(PO_4)_2{\cdot}+16{\cdot}NH_4NO_3{\cdot}+{\cdot}6{\cdot}H_2O \quad (3)$$

where x = 0.2; 0.4; 0.6.

Calcium-magnesium phosphate powders with the ratio (Ca + Mg)/P of 1.5, 1.67 and 2 with the degree of substitution of Mg for Ca 20, 40 and 60 mol. % were used as the cement powders, the composition and labels are listed in Table 1 and presented in Fig. 1. When we produced the cements based on the cement powders, the label changed from CP/MCP to CPC/MCPC. The powder with Ca/P = 2 and 0 mol.% of Mg (CP) was chosen as control sample as pure calcium-phosphate powder which could interact with NaH_2PO_4 cement liquid with a formation of set cements. The pH of the reaction mixture has been maintained at a level of 7–8 by adding aqueous ammonia.

The powder precursors were synthesized by simultaneous addition of $Ca(NO_3)_2$ and $Mg(NO_3)_2$ solutions into $(NH_4)_2HPO_4$ solution with constant stirring. After the mixing, the suspensions were evaporated to obtain the powder precursors keeping the chemical composition including excesses of cations. The powders precursors were air dried, heat-treated at 300 °C for 6 h to remove of NH_4NO_3. The powders precursors were calcinated at 1150 °C in air for 2 h to allow the formation of crystalline phases. The sintered blocks were ground in an agate mortar and milled in a planetary ball mill for 20 min with the isopropyl alcohol medium with zirconia balls. Cement powders were air

Table 1
Powders assignments and particle size distributions.

Cement powder composition name	(Ca + Mg)/P ratio	Mg subst., mol.%	Particle size distribution		
			D_{10} (μm)	D_{50} (μm)	D_{90} (μm)
MCP1	1.5	20	4.1	28.1	54.4
MCP2	1.5	40	2.8	24.3	49.9
MCP3	1.5	60	5.5	31.5	63.8
MCP4	1.67	20	1.0	15.4	51.7
MCP5	1.67	40	1.2	17.7	47.8
MCP6	1.67	60	11.5	41.1	89.9
MCP7	2.0	20	0.9	6.7	19.3
MCP8	2.0	40	1.0	7.9	21.6
MCP9	2.0	60	1.3	10.0	35.5
CP	2.0	0	0.5	17.7	35.4

dried and characterized. The particle size distribution was measured by laser diffraction (FRITSCH ANALYSETTE 22). The powder materials were characterized by the X-ray diffraction (XRD) method (Shimadzu XRD-6000 or Dron III, CuKα radiation, 2θ range from 10 to 70° with a step of 0.02°) with the identification of phase composition according to ICDD PDF2 database. Quantitative phase analysis was performed according to the technique described in Ref. [20]. The procedure is based on the Rietveld method and uses the PHAN% software developed at the Department of Physical Material Science, National Research Technological University. The accuracy of phase amount determination was up to 3%. Indexing of the peaks was carried out by means of cards JCPDS No 25–1137 for (TeTCP), JCPDS No 09–0432 for (HA), JCPDS No 87–1582 for magnesium –substituted whitlockite phase ($(Ca_{2,586}Mg_{0,411})(PO_4)_2$), JCPDS No 77–2364 for stanfieldite ($Mg_3Ca_3(PO_4)_4$), JCPDS No 77–2364 for (MgO), JCPDS No 70–2065 for whitlockite (β-$Ca_3(PO_4)_2$), JCPDS No 75–1714 for newberyite ($MgHPO_4*3(H_2O)$), JCPDS No 72–0713 for brushite ($CaHPO_4*(2H_2O)$), JCPDS 33-878 for bobierrite ($Mg_3(PO_4)*8H_2O$). Fourier-transform infrared absorption (FTIR) spectra of the samples were measured in KBr pellets in the range from 4000 to 400 cm^{-1} employing a Nikolet Avatar-330 FTIR spectrometer. Morphology of powders was investigated by scanning electron microscopy (SEM, Tescan Vega II) with X-ray energy dispersive spectroscopy (EDS, Inca, Oxford Instruments).

2.2. Preparation and characterization of the cement samples

The solution based on 50 wt.% NaH_2PO_4 with pH 4.0 ± 0.1 was used as cement liquid. The powders and the liquid were mixed, and the obtained cement pastes were placed into a teflon molds (d = 5 mm, h = 10 mm) and hardened for 48 h at 37 °C and 100% humidity. The final setting time was determined by immersing a Vicat needle with a diameter of 1.0 mm of indenter (400 g) into the sample being set until the needle could no longer form a complete circular indentation on the cement according to ISO 9917 (2007).

The chemical composition of the set cements was investigated by inductively coupled plasma atomic emission spectrometry (ICP-AES) analysis. Sample preparation included the transfer of weighed portion of the dried and milled substance (75–120 mg) to a 100 ml conical flask and further dissolving of the sample by addition of 25 ml of aqua regia (3:1 by volume of concentrated hydrochloric and nitric acid). The flask was heated for 10 min at 90 °C until completely sample dissolved; then, the solution was placed into 50 ml volumetric flask, deionized water added to the mark. Before ICP-AES analysis, a 10-fold dilution of the samples was performed. A standard reference solution of Na, Mg, Ca, and P (Merck, Germany) was used. Internal standard (20 ppm of Sc in 5 mass.% HNO_3) was used to improve the reproducibility of the results. In all cases, two parallel samples were analyzed to check the reproducibility of the replicates. For elements weight determination the wavelength used: 330.237 (I), 588.995 (I), 589.592 (I) nm for Na, 285.213 (I) and 279.078 (II) for Mg, 315.887 (II) and 317.933 (II) for P, 213.618 (I) and 214.914 (I) for Sc (internal standard).

Samples obtained after hardening were investigated by XRD and FTIR by the procedures identical to those used for cement powders. The compressive strength of dry hardened cement samples was determined according to ASTM D695-91 standard test with an Instron 5581 machine under uniaxial compression with a loading speed of 1 mm/min (error in measuring speed 0.2%, error in measuring load 0.5%) and the final statistical calculations were carried out for 5 samples.

The set cements were placed in deionized water and Kokubo's simulated body fluid (SBF) [21] at the ratio of 0.2 g/ml and pH values of the extracts were determined after 1, 24 and 72 h of cements incubating. The results were expressed as the average pH value standard deviation (SD). The SBF was prepared by dissolving NaCl, $NaHCO_3$, KCl, $K_2HPO_4*3H_2O$, $MgCl_2*6H_2O$, $CaCl_2$ and Na_2SO_4 in deionized water in adjusted ratio (Table 1). The solution was buffered at pH 7.4 with tris(hydroxymethyl) aminomethane ($(CH_2OH)_3CNH_2$, TRIS) and 1 M HCl. Microstructure of the set cements was evaluated by SEM.

2.3. Measurement of the degradation rate in the simulated body fluid (SBF)

The degradation rates of the samples were characterized by their weight loss ratios after immersion in SBF solution at 37 °C [16]. For determination of the weight loss, 3 samples for each composition were prepared and hardened during 48 h and initial weight was recorded. Then samples were immersed in the separate plastic bottle for each sample into the SBF solution with a weight-to-volume ratio of 0.2 g/ml. After 1, 3, 7, 14 and 21 days of solubility at 37 °C in closed system the samples were removed from the SBF solution, frozen by ULT Freezer MDF-60U50 up to −70 °C and freeze-dried by LS-1000 Prointeh-bio with sublimation capacitor. After freeze-drying new weight, W_t, was

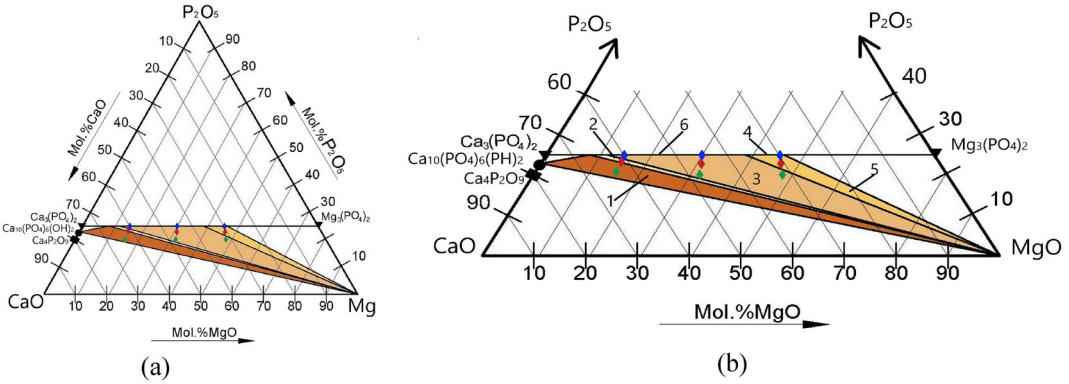

Fig. 1. The ternary phase diagram CaO–MgO–P_2O_5 at 1000 °C (a) with mentioned compositions of cement powders and phase areas according to Ref. [23] (b): MCP1-3 (blue diamond), MCP4-6 (red diamond), MCP7-9 (green diamond), CP ($Ca_4P_2O_9$) – black square, the areas are listed below in Table 2.

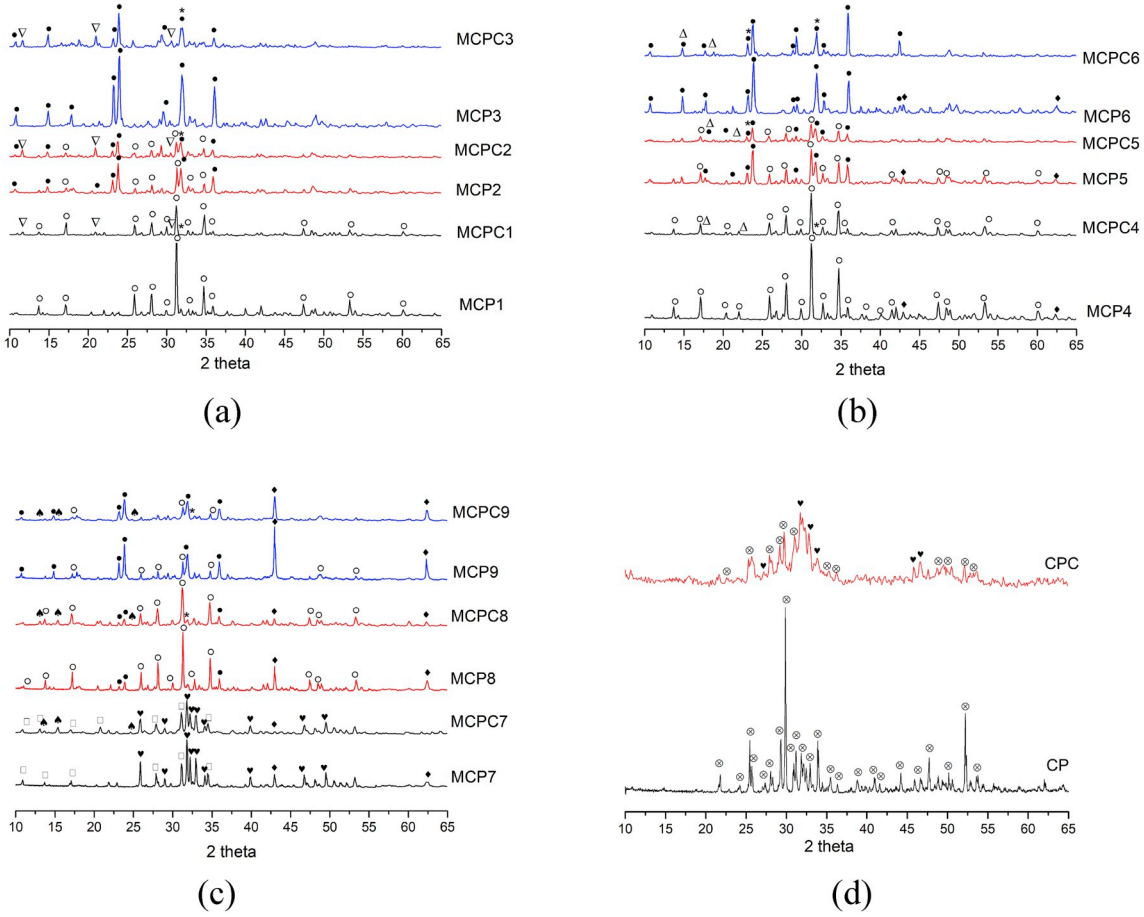

Fig. 2. Diffractograms of the cement powders/set cements after 48 h of hardening: (Ca + Mg)/P = 1.5(MCP/MCPC1-3) (a), (Ca + Mg)/P = 1.67(MCP/MCPC 4–6) (b), (Ca + Mg)/P = 2.0 (MCP/MCPC 7–9) (c) and initial CP and CPC (d), where ● – stanfieldite, ▫ - whitlockite (β-$Ca_3(PO_4)_2$), ○ – whitlockite (($Ca_{2,586}Mg_{0,411}$)$(PO_4)_2$), ♥ - HA, ♦ - MgO, ♠ - $MgNa(PO_4)$*$7H_2O$, ⊗ - TeTCP, Δ – newberyite, ▽ - brushite, * -Na_2HPO_4.

Table 2
Diagram characteristics and phase compositions of the obtained cement powders according to XRD.

Area on the diagram	Phases on the area according to [23]	Cement powders	Phase composition, wt.%			
			Hydroxyapatite	Whitlockite	Stanfieldite	MgO
1	HA, Whitlockite, MgO	MCP7	55	28	–	15
2	Whitlockite, MgO	MCP4	–	85	–	15
3	Whitlockite, Stanfieldite, MgO	MCP5	–	18	75	7
		MCP8	–	62	9	28
		MCP9	–	17	34	49
4	Stanfieldite	MCP3	–	–	100	–
5	Stanfieldite, MgO	MCP6	–	–	93	7
6	Stanfieldite, Whitlockite	MCP1	–	85	15	–
		MCP2	–	10	90	–

recorded and weight changes was determined.

For determination of Mg and Ca release during the immersion in the SBF solution, extracts were taken after 1, 3, 7, 14 and 21 days of soaking and analyzed by atomic emission spectrometry with inductively coupled plasma (AES-ICP, HORIBA Jobin Yvon, ULTIMA 2) or ICP-OES Agilent 720. Scandium line (335.372 nm) 20 mg/l was used to improve reproducibility. Calibration solutions were prepared using single-element standard samples (Inorganic Ventures, USA). To control the quality of the results standard samples (ICP-MS Quality Control Standards, Inorganic Ventures) were used. Before measurements the optimal measurement conditions was obtained according to the following parameters (power, plasma flow, additional flow, read time for replicates, stabilization time, replicates).

2.4. Determination of cell proliferation and morphology

In vitro cytocompatibility of cement samples was investigated by using MTT assay on the cell line of human osteosarcoma MG-63 (Russian Collection of Cell Cultures, Institute of Cytology, Russian Academy of Sciences, St. Petersburg). Before the start of *in vitro* studies, MCPC and CPC samples were sterilized with γ-radiation at a dose of 18 kGy. Sterile cement disk samples 5.0 mm diameter and 3.0 mm high were placed into 96- well plates for cultivation (Corning Costar, USA) into triplets with one plate per each incubation period and covered with complete growth medium (CGM) that contained DMEM medium (PanEco, Russia), 10% fetal bovine serum (PAA, Austria), 60 mg/ml -glutamine (PanEco, Russia), 20 mM Hepes buffer (PanEco, Russia) and

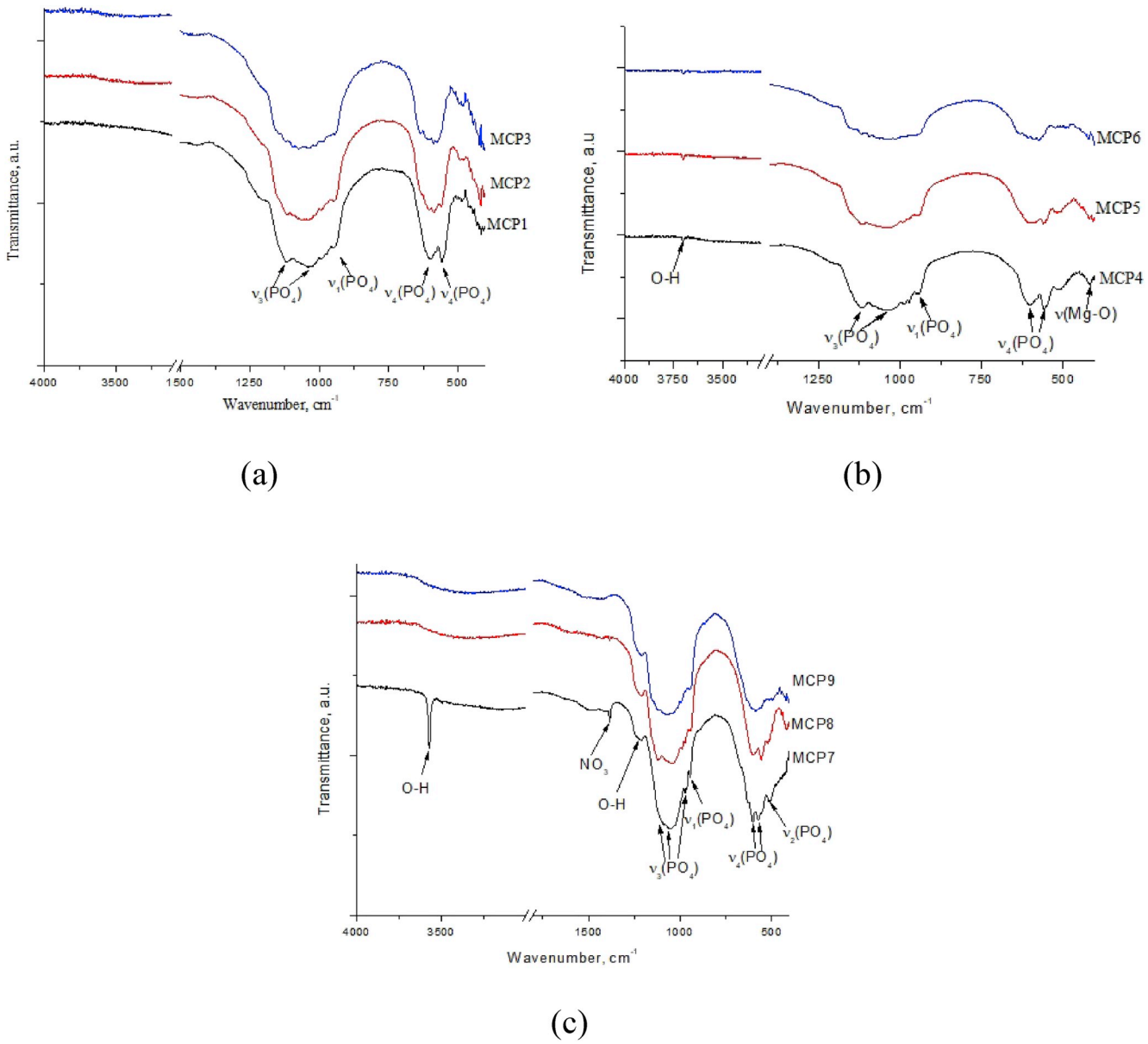

Fig. 3. FTIR spectra of the cement powders: (Ca + Mg)/P = 1.5 (MCP1-3) (a); (Ca + Mg)/P = 1.67 (MCP4-6) (b); (Ca + Mg)/P = 2.0 (MCP7-9) (c).

50 μg/ml gentamycin (PanEco, Russia) for 4–6 h for samples soaking. After the medium was removed from wells using a pipette, and 200 μl of MG-63 suspension in the fresh CGM containing 1.5×10^4 cells per well was added, the suspension containing 7.5×10^4 cells per 1 ml was applied. The plates were incubated for 1, 3, 7, 10 and 14 days with regular replacements of the CGM. All the procedures were performed under sterile conditions in an atmosphere of moist air that contained 5% CO_2 at 37 °C. The viability of MG-63 cell lines over time was assessed using an MTT test [22], which is based on the ability of dehydrogenase of living cells to reduce 3- (4,5-dimethyl-2-thiazolyl)-2,5-diphenyl-2h-tetrazolium bromide (MTT, (Sigma), USA) into formazan. The optical density of the formazan solution was evaluated spectrophotometrically on a spectrophotometer Multiscan FC (Thermo Scientific, USA) at a wavelength of 540 nm. It is known that the amount of formazan describes proliferative activity (viability and amount) of different human and animal cells [22]. The pool of viable cells (PVC) was evaluated at different stages of the experiment as a ratio of optical density of formazan solution on a certain day of the experiment to optical density in the control. A specimen of cement was assumed to be cytocompatible in the absence of cytotoxicity (PVC ≥ 70%) on a certain day of cultivation. At the stages of the experiments, visual monitoring of the processes of expansion of the surface of cement samples by cells was carried out and photo archiving of materials (stereo magnifier Olympus, Japan).

The obtained results were processed by conventional methods of variational statistics using Microsoft Excel 2000. The significance of differences was assessed using a parametric Student t-test; differences were considered statistically significant at $p < 0.05$.

3. Results and discussion

3.1. Cement powders characterization

3.1.1. Phase compositions of the cement powders

According to XRD data, the compositions of cement powders with (Ca + Mg)/P = 1.5 ratio form whitlockite and stanfieldite phases (Fig. 2), which belong to the same structural type and differ mostly in Ca/Mg ratio. The MCP1 (20 mol.% Mg) composition is mostly trigonal whitlockite with traces of monoclinic stanfieldite. The increase of Mg content resulted in a progressive increase of stanfieldite content

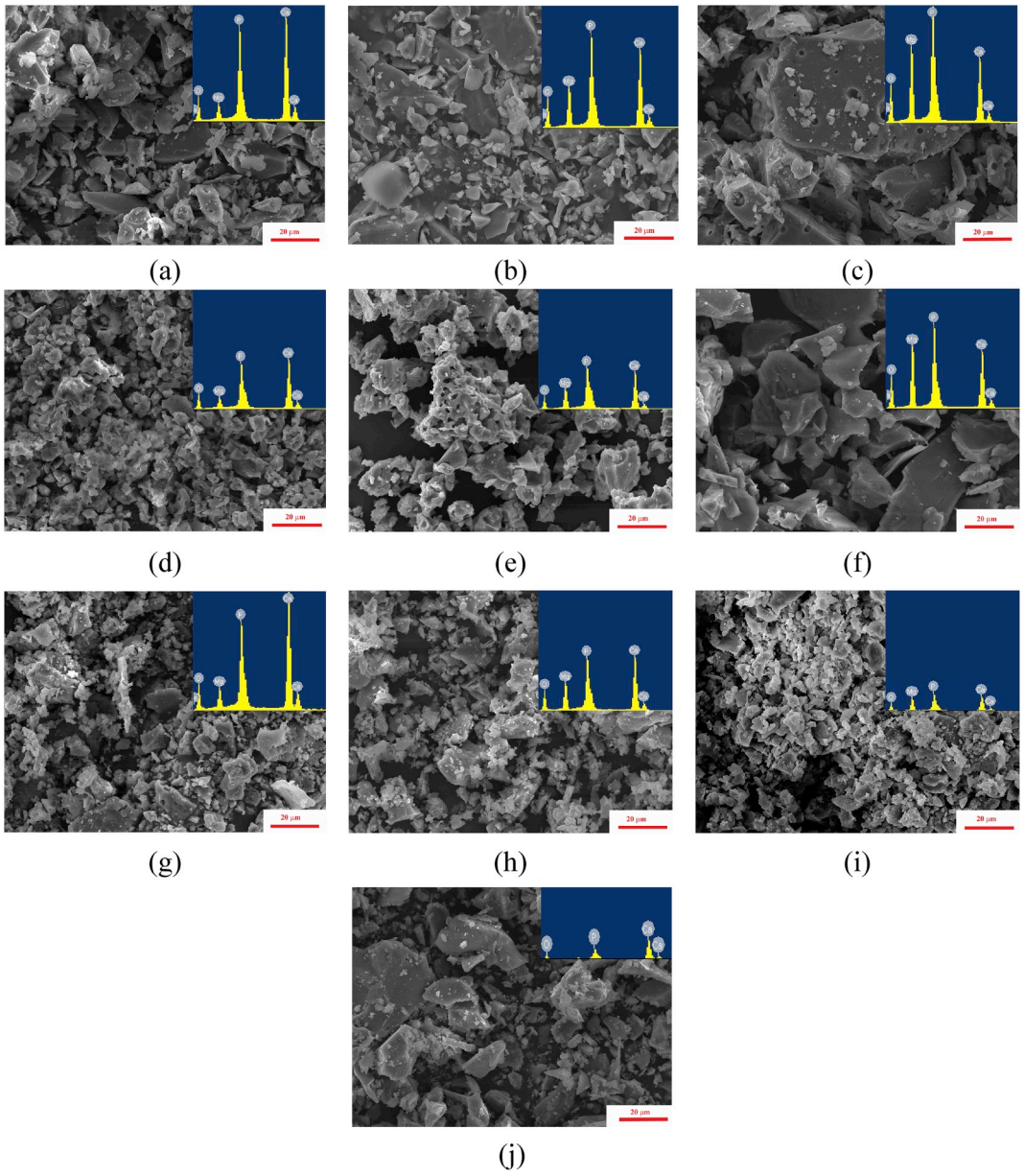

Fig. 4. The morphology and EDX spectra of the cement powders: MCP1 (a); MCP2 (b); MCP3 (c); MCP4 (d); MCP5 (e); MCP6 (f); MCP7 (g); MCP8 (h); MCP9 (i) and CP(j).

reaching pure stanfieldite phase at 60 mol.% of Mg (MCP3) (Table 1, Fig. 1)..

The increase of (Ca + Mg)/P ratio up to 1.67 resulted in the formation of additional MgO phase, with its amount below 15 wt.%, depending on the specific composition. MCP4 (20 mol.% Mg) contains predominantly whitlockite phase with ~15 wt.% MgO. MCP5 (40 mol.% Mg) and MCP6 (60 mol.% Mg) are predominately stanfieldite with ~7 wt.% of MgO and small amount of whitlockite in MCP5. So, the evolution of phase composition (whitlockite to stanfieldite transformation) is qualitatively similar between the two series of samples with different (Ca + Mg)/P ratio. The further increase of (Ca + Mg)/P ratio to 2.0 resulted in the formation of HA in the case of MPC7 (20 mol.% of Mg) with whitlockite and MgO phases. The increase of Mg content resulted in the disappearance of HA and the formation of mixtures of stanfieldite, whitlockite and MgO phases. The CP (0 mol.% Mg) was single-phase TeTCP (Fig. 5 d). The results of XRD were compared with phase diagram of MgO–CaO–P_2O_5 system at 1000 °C, where single-phase area of stanfieldite covers a broad composition range between 45 and 65 mol.% of Mg (Fig. 1) [23]. We observed up to 90 wt.% of stanfieldite phase in the case of 40 mol.% Mg (MPC2), which is consistent with these data (Table 2). The presence of HA phase is also consistent with the phase diagram at high (Ca + Mg)/P ratio (MCP7), however HA remained undetected at lower (Ca + Mg)/P (MPC4).

3.1.2. FTIR spectra of the cement powders

The FTIR spectra of cement powders are presented in Fig. 3. The FTIR spectra of powders at the (Ca + Mg)/P = 1.5 ratio (Fig. 3a) were presented by well resolved bands of phosphate group at 570, 602, 1034 and 1086 cm^{-1} [24]. It should be noted, that as the magnesium content in the materials increases, the doublet of the deformation mode v_3 PO_4^{3-} at 1119 and 1035 cm^{-1}, which is characteristic of the whitlockite phase [25], becomes less resolved and transforms into a broad peak with a maximum at 1040 cm^{-1}, which we could associated with formation of pure stanfieldite phase. Also, at low wavenumbers the doublet of v_4 PO_4^{3-} at 602 and 560 cm^{-1} previously attributed to Mg-substituted whitlockite [26] demonstrated the decrease of intensity

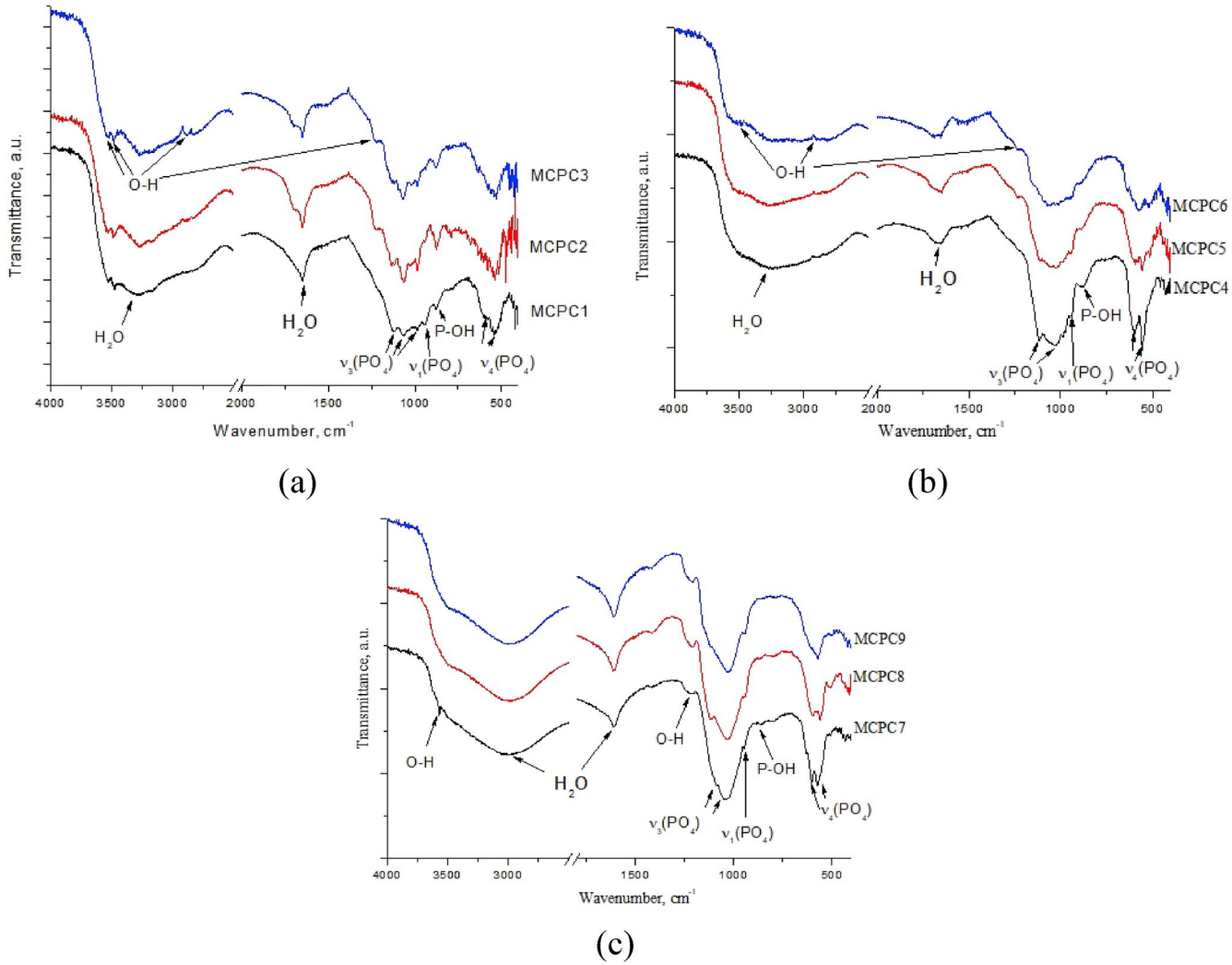

Fig. 5. FTIR spectra of the set cements: (Ca + Mg)/P = 1.5 (MCPC1-3) (a); (Ca + Mg)/P = 1.67 (MCPC4-6) (b); (Ca + Mg)/P = 2.0 (MCPC7-9) (c).

with the growth of Mg content which results in formation of the single broad peak with maximum at 576 cm^{-1} for MCP3 sample. The new peak of PO_4^{3-} associated with stanfieldite formation was observed at 633 cm^{-1} and the same behavior was observed for MCP6.

In the same time, the increase of the (Ca + Mg)/P ratio of up to 1.67 (Fig. 3b) resulted in the appearance of OH^- band at 3700 cm^{-1}. This band is attributed to $Mg(OH)_2$, which formed by interaction of MgO with air humidity [27].The behavior of the doublet of the ν_3 PO_4^{3-} at 1119 and 1035 cm^{-1} with increase of Mg content reflected the disappearance of whitlockite phase according to XRD and resulted in a formation of broad peak at 1040 cm^{-1} similar to (Ca + Mg)/P = 1.5 system. At the same time, the band of the stretching mode ν_1 of the PO_4^{3-} group becomes less resolved at 951 cm^{-1} and disappeared for MPC6. The doublet of the deformation mode ν_4 at 557 and 605 cm^{-1} becomes smoother and forms a single maximum at 571 cm^{-1}, and the ν_2 bands are shifted toward large wave numbers from 512 to 526 cm^{-1}.

Regardless neither Mg content, nor whether MgO forms as separate phase or not according to XRD, the only well-resolved peak at 420 cm^{-1} associated with Mg–O vibration [28] was observed for all samples.

For (Ca + Mg)/P = 2.0 ratio, ν_2 (508 cm^{-1}), ν_3 (1088, 1050, 973 cm^{-1}) and ν_4 (604, 571 cm^{-1}) PO_4^{3-} bands are clearly observed (Fig. 3c). Narrow O–H band at 3570 cm^{-1} related to OH group in hydroxyapatite was observed only in MCP7 sample, but not in MCP4, consistent with XRD observations [25]. The weak band at 1213 cm^{-1} can be ascribed to the O–H in-plane bending [29]. For MCP7, bending mode related to NO_3 group appears at 1380 cm^{-1} [25].

3.1.3. Particle size distribution, morphology and EDX results

The size distributions of obtained cement powders particles according to laser diffraction were in the 22–35 μm range and are listed in Table 1. The data were in agreement with SEM results presented in Fig. 4. The particles had an irregular shape with predominantly sharp edges. A significant growth of particle size was observed with increase of Mg content. It could be attributed to the formation of a mechanically stronger stanfieldite phase and consequently, lower degree of milling in the case of 60 mol.% of Mg substitution. According to EDX data the ratio of (Ca + Mg)/P changed closed to predicted from nominal compositions (Table 3).

3.2. Cements characterization

3.2.1. Powder to liquid ratio, setting time, element composition

To produce the cement samples, we used the powders to liquid ratio of 1.5–2.0 g/ml in the case of MCPC and 1.0 g/ml for CPC as presented in Table 3. For MCPC1-6 it was 2.0 and independent on composition, but in the case of MCPC7-9 the volume of the liquid was increased due to high amount of MgO and presence of the inert HA in the case of MCPC7.

Cement materials MCPC are characterized by setting time which is

Table 3
Cements samples properties and compositions.

Composition	(Ca + Mg)/P cement powders ratio	(Ca + Mg)/P cement powders ratio according to EDX	Optimum P/L (g/ml)	Setting time, min	Ca, wt.% according to ICP	Mg, wt.% according to ICP	P, wt.% according to ICP	Na, wt.% according to ICP	Mg substitution theoretical, mol. %	Mg substitution experimental, mol. %	(Ca + Mg)/P	(Ca + Mg + Na)/P
MCPC1	1.5	1.6	2	27(1)	27.58 (0.69)	4.32 (0.11)	20.8 (0.2)	3.53 (0.09)	20	21 (0.03)	1.29	1.52
MCPC2	1.5	1.6	2	25(1)	20.87 (0.52)	9.08 (0.23)	20.2 (0.51)	3.60 (0.09)	40	42 (0.03) 1,381,38	1.38	1.62
MCPC3	1.5	1.5	2	20(1)	16.22 (0.41)	14.49 (0.36)	20.7 (0.52)	2.81 (0.07)	60	60 (0.03)	1.52	1.70
MCPC4	1.67	1.7	2	17(1)	29.28 (0.73)	4.41 (0.11)	20.7 (0.52)	3.36 (0.08)	20	20 (0.03)	1.37	1.59
MCPC5	1.67	1.7	2	16(1)	23.34 (0.58)	10.42 (0.26)	19.9 (0.50)	3.00 (0.07)	40	43 (0.03)	1.58	1.79
MCPC6	1.67	1.7	2	13(1)	17.27 (0.43)	15.32 (0.38)	20.1 (0.50)	3.11 (0.08)	60	60 (0.03)	1.65	1.86
MCPC7	2.0	2.1	1.7	15(1)	32.34 (0.81)	4.73 (0.12)	18.8 (0.47)	4.35 (0.11)	20	20 (0.03)	1.66	1.97
MCPC8	2.0	2.1	1.7	9(1)	24.15 (0.60)	9.53 (0.24)	19.0 (0.48)	5,00 (0,12)	40	40 (0.03)	1.63	1.99
MCPC9	2.0	2.0	1.5	6(1)	16.84 (0.42)	14.24 (0.36)	19,5 (0.49)	4,98 (0,12)	60	58 (0.03)	1.61	1.96
CPC	2.0	2.0	1.0	2(1)	27.73 (0.69)	< 0.05 (−)	18.9 (0.47)	8,13 (0,20)	0	< 0.05 (−)	1.14	1.71

close to optimal for cement handling (5–30 min) The materials with (Ca + Mg)/P = 1.5 ratio showed the setting time in the range of 27 to 20 min, which decreased with the growth of Mg content. The cements with (Ca + Mg)/P = 1.67 are characterized by shorter setting timedue to the presence of highly active MgO in the cement powders. The materials with (Ca + Mg)/P = 2.0 demonstrated the setting time lower than 10 min due to high concentration of MgO, as it is described in Ref. [6]. CPC characterized by the lowest setting time – 4 min and required the highest powder/liquid ratio – 1.0 g/ml (Table 3).

ICP results confirmed that the substitution degree of Mg as defined by the composition of powders was preserved in set cement samples (Table 4). During the interaction with cement liquid and setting the cement samples demonstrated the decrease of (Ca + Mg)/P ratio linked with the amount of Mg in the sample. With the increase of Mg content, both (Ca + Mg)/P and (Ca + Mg + Na)/P ratio values increased in MCPC1-6 following lower atomic weight of Mg compared to Ca, while same weight quantity of cement powder and setting liquid was used for all samples. The (Ca + Mg)/P and (Ca + Mg + Na)/P ratio changed insignificantly with nominal Mg content in the case of MCPC7-9 due to cancellation of contributions from P/L ratio and atomic weight difference.

3.2.2. Phase composition of the set cements

According to XRD, the diffraction peaks of initial phases became broadened after the cement setting indicating a significant decrease in the degree of crystallinity (Fig. 2). The new phases which appear as a result of material's interaction with the cement liquid for MCPC1-MCPC3 are newberyite and brushite. We supposed the formation of Na_2HPO_4 (JCPDS # 35–0735) with the main peaks at 31,87; 32,77 and 23,14; which overlapped with ones of the stanfieldite and whitlockite phases as a residual of cement liquid. Also, we assumed the introduction of Na^+ into whitlockite and stanfieldite structure, as it was described by us previously [15]; related compositions had been also reported earlier e.g. as $Ca_9MgNa(PO_4)_7$ (JCPDS # 45–0136). Thus, we have established the selective formation of new magnesium – phosphate (newberyite) and calcium – phosphate (brushite) phases during the formation of cement materials (Fig. 2 a). The amount of brushite decreased with increasing of magnesium content in the materials from 25 wt.% for MCPC1 to 10 wt.% for MCPC3. The chemical processes could be summarized by a scheme (4):

$$(Ca_{2,586}Mg_{0,411})(PO_4)_2\cdot + \cdot Ca_3Mg_3(PO_4)_4 + (2 + w + z)NaH_2PO_4\cdot \rightarrow \cdot(Ca_{2,586}Mg_{0,411})_{(1-w/2)}(Na_w)(PO_4)_2\cdot + \cdot(Ca_{(3-x)}Mg_{(3-y)})_{(1-z/2)}Na_z(PO_4)_4\cdot + \cdot xCaHPO_4^*2H_2O\cdot + \cdot + yMgHPO_4^*3H_2O\cdot + \cdot Na_2HPO_4\cdot,\cdot(\ x > y) \quad (4)$$

During the interaction of MCPC4-MCPC6 with cement liquid the diffraction peaks of MgO disappeared (Fig. 2 b). This could be attributed to simultaneous dissolution of calcium-magnesium phases and MgO in the cement liquid with the formation of crystalline newberyite. The formation of brushite was not detected.

Cements phase formation of materials with (Ca + Mg)/P = 2.0 ratio is mostly associated with the formation of $NaMgPO_4{*}7H_2O$ phase [30] via the interaction of MgO with cement liquid according to reaction:

$$MgO + NaH_2PO_4 + 6H_2\ O = NaMgPO_4^*7H_2O \quad (5)$$

Neither newberyite nor brushite phases were detected by XRD (Fig. 2 c). For MCPC7 the amount of HA changed insignificantly indicating its low reaction activity. Significant amount of residual MgO was observed in MCP8 and MCP9 samples, consistent with its high content in the initial materials. Transformation of TeTCP into HA was observed in the case of CPC: the HA content in the final material was up to 60 wt.% (Fig. 2 d).

Table 4
The characteristics of the set cements.

Composition	Compressive Strength, MPa	pH value in distillated water			pH value in SBF solution		
		1 h	24 h	72 h	1 h	24 h	72 h
MCPC1	2(1)	6.8(0.05)	7.1(0.05)	7.2(0.05)	7.4(0.05)	7.4(0.05)	7.5(0.05)
MCPC2	3(1)	6.8(0.05)	7.1(0.05)	7.2(0.05)	7.5(0.05)	7.5(0.05)	7.5(0.05)
MCPC3	6(2)	6.9(0.05)	7.1(0.05)	7.3(0.05)	7.5(0.05)	7.5(0.05)	7.5(0.05)
MCPC4	22(3)	7.3(0.05)	7.3(0.05)	7.3(0.05)	7.6(0.05)	7.6(0.05)	7.6(0.05)
MCPC5	15(2)	7.1(0.05)	7.1(0.05)	7.2(0.05)	7.6(0.05)	7.6(0.05)	7.6(0.05)
MCPC6	16(2)	7.2(0.05)	7.2(0.05)	7.2(0.05)	7.6(0.05)	7.6(0.05)	7.6(0.05)
MCPC7	30(2)	7.8(0.05)	9.0(0.05)	9.5(0.05)	8.3(0.05)	8.0(0.05)	8.0(0.05)
MCPC8	34(3)	7.8(0.05)	9.0(0.05)	9.6(0.05)	8.1(0.05)	8.2(0.05)	8.4(0.05)
MCPC9	41(3)	7.9(0.05)	9.1(0.05)	9.8(0.05)	8.2(0.05)	8.3(0.05)	8.5(0.05)
CPC	18(2)	7.8(0.05)	8.0(0.05)	9.1(0.05)	8.2(0.05)	7.9(0.05)	8.1(0.05)

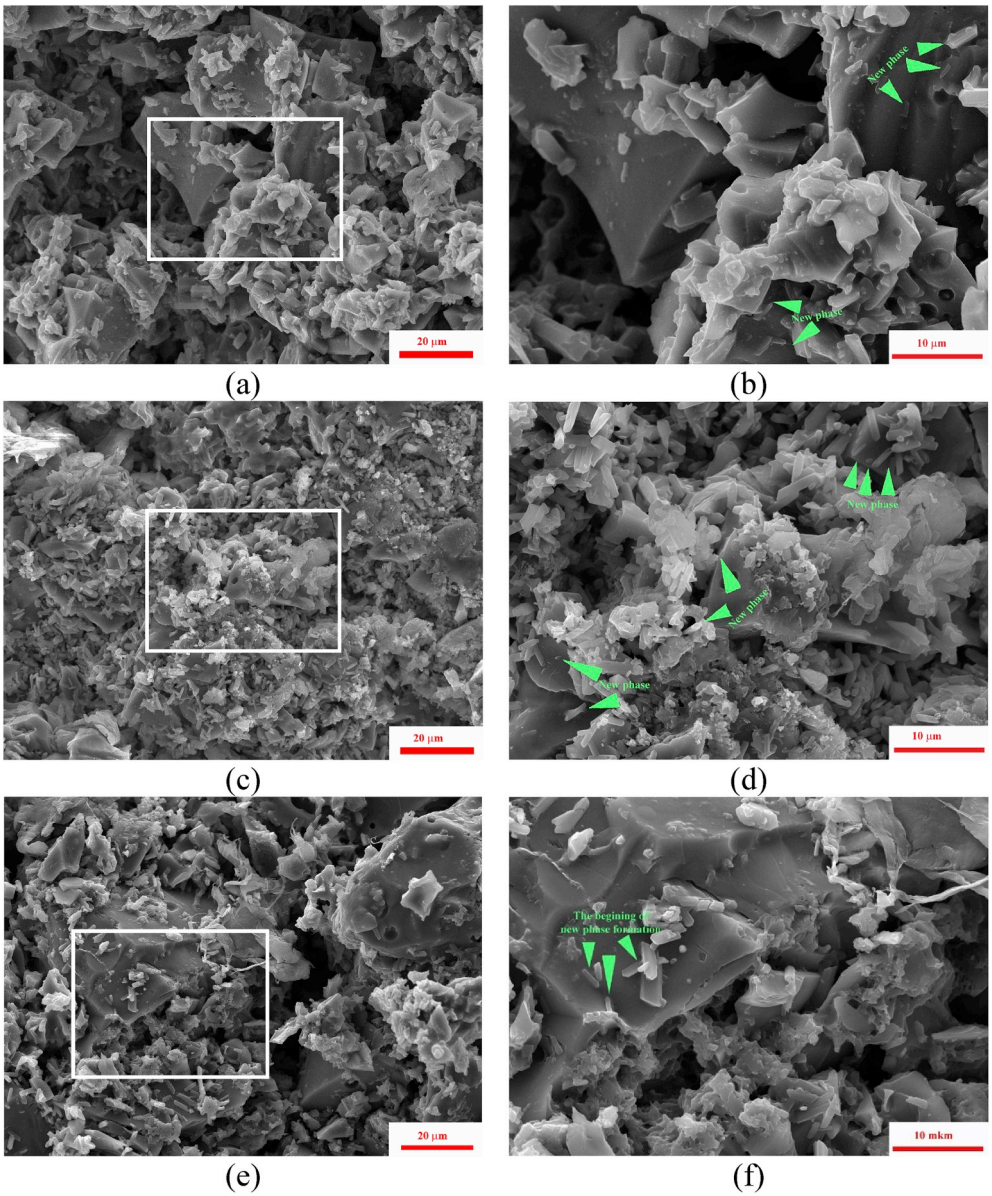

Fig. 6. Microstructure of the set cements: MCPC1 (a,b); MCPC2 (c,d); MCPC3 (e,f); green arrows indicates the new phase areas.

3.2.3. FTIR spectra of the set cements

The IR spectroscopy analysis confirmed the formation of crystal hydrates during the reaction of cement powders with cement liquid (Fig. 5).

Compared with the IR spectra of cement powders, the IR spectra of set cements showed wide and intense bands of adsorbed water at 3600-2500 cm^{-1} and at 1600-1610 cm^{-1}. For MCPC7, the additional band of structural OH^-group at 3550 cm^{-1}, related to HA still may be

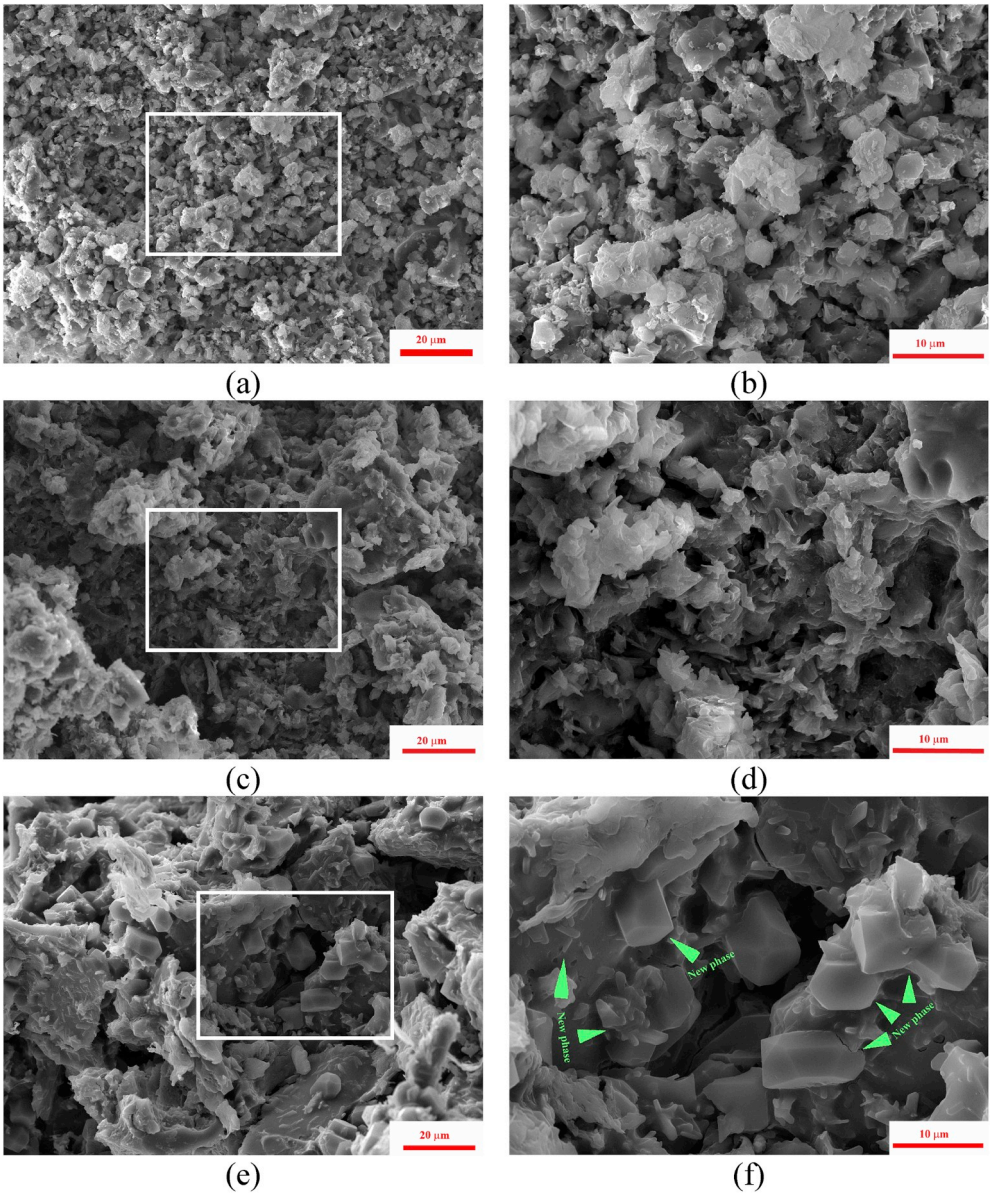

Fig. 7. Microstructure of the set cements: MCPC5 (a,b); MCPC6 (c,d); MCPC7 (e,f); green arrows indicates the new phase areas.

recognized (Fig. 5 c), while no bands which could be related to Mg $(OH)_2$ was observed. After interaction with the cement liquid, the P–OH band at 875 cm^{-1} related to HPO_4^{2-} group appear in all cement samples, while the ν_2 band of PO_4 (usually present at 510 cm^{-1}) is difficult to distinguish [31]. The appearance of P–OH band can be referred to newly formed brushite and newberyite phases observed by XRD. The presence of newberyite phase is further evidenced by the OH-group stretching vibrations bands at 3163, 3267, and 3636 cm^{-1} for MCPC1-3 of the three nonequivalent H_2O molecules in the newberyite structure (Fig. 5 a) [13]. Also, bands at 2920 and 2850 and 2400 cm^{-1} attributed to stretching vibrations of strong H-bonding of OH of newberyite H_2O molecules [13] became distinguishable for MCPC2 and MCPC5 with 40 mol.% of Mg, and increase in their intensity with the increase of Mg concentration (Fig. 5 b). This confirmed the XRD data on the formation of hydrated phase of newberyite in MCPC3 and MCPC6. Also, an overall tendency for (Ca + Mg)/P = 1.5 and (Ca + Mg)/P = 1.67 cements was the decrease of intensity of ν_1 PO_4^{3-} at 945 cm^{-1} and the doublet of the mode ν_2 PO_4^{3-} at 510–520 cm^{-1} with an increase in magnesium concentration from 20 to 60 mol.% associated with a transformation of whitlockite structure into stanfieldite one.

Although for MCPC7-9 samples the P–OH band nearly disappears, the disturbance in the range 880-860 cm^{-1} may indicate amorphous phase formation. Also, the new band of OH-group was detected at 1210 cm^{-1} which could be attributed to the formation of $MgNaPO_4$*$7H_2O$. The shape of ν_3 PO_4 (at 1100-970 cm^{-1}) bands also changes with the material composition. For samples MCPC1-3 three separate bands can be clearly distinguished, while with the growth of (Ca + Mg)/P ratio, these bands become less resolved. This fact may indicate greater amorphization of the set cements with the growth of (Ca + Mg)/P ratio.

3.2.4. Microstructure of the set cements

The cement samples demonstrated an increase of density and decrease of porosity with the growth of (Ca + Mg)/P ratio. The new-formed phase was observed for all MCPC samples in the form of small lamellas and rods which formed a network between the particles of the initial cement powders (Fig. 6 a-f).

The MCPC1 sample is characterized by a loose and porous structure with pores ranging from 1 to 2 to 6–8 μm; the increase of Mg content resulted in a denser structure in MCPC3. Rod-shaped crystals with the

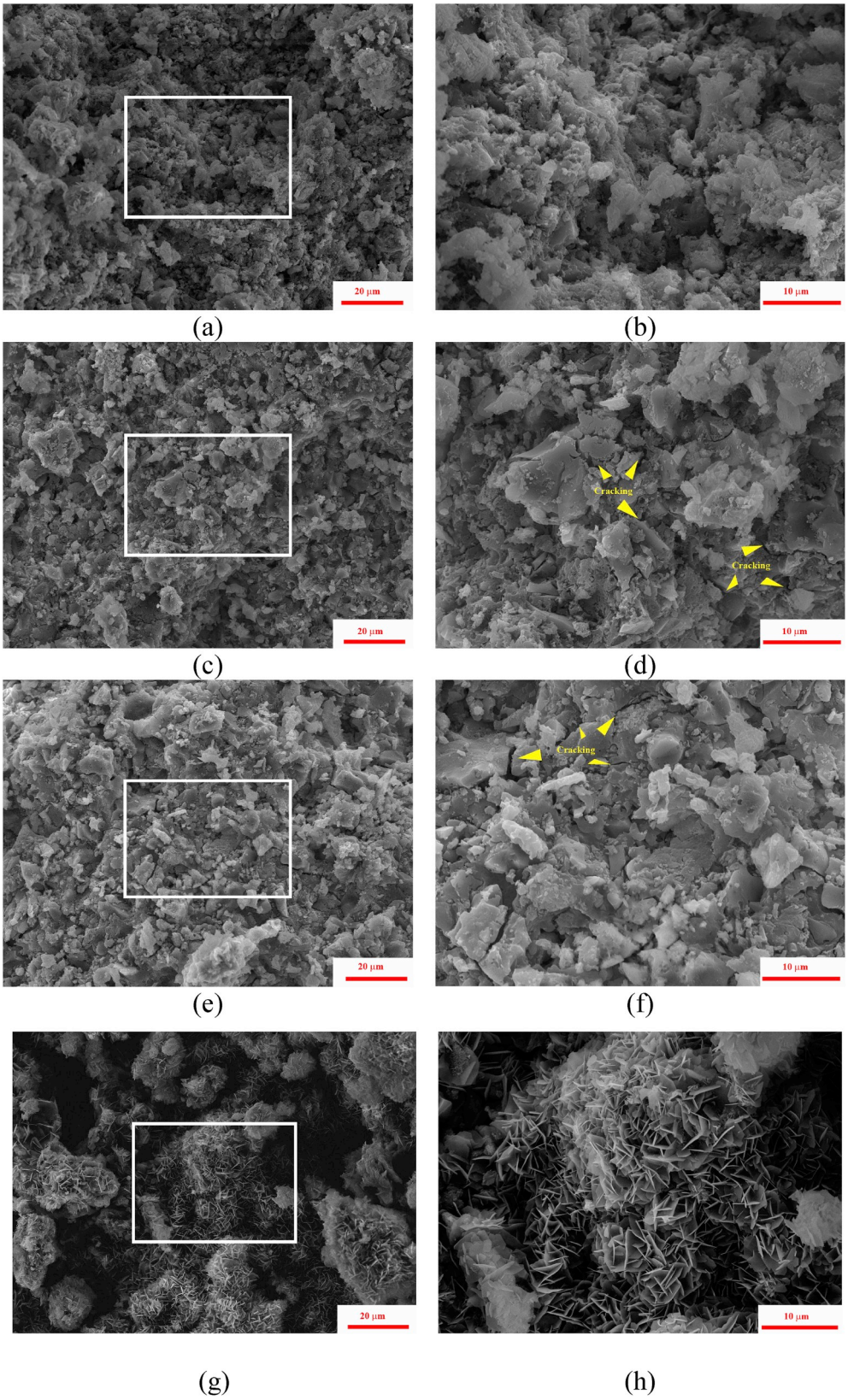

Fig. 8. Microstructure of the set cements: MCPC7 (a,b); MCPC8 (c,d); MCPC9 (e,f); CPC (g,h); yellow arrows indicates the cracking occurs.

size of 0.5–5 μm are grown on the surface of the initial cement powders (with 15–40 μm in size) and network structure by brushite and newberyite formed during setting and hardening of cement. Additionally, newberyite crystals were observed on the surface of the initial cement powders in the cements with (Ca + Mg)/P = 1.67 ratio (Fig. 7 a-f).

The porosity decreased with Mg content increase, and the samples microstructure became denser. The formation of significantly enlarged prismatic crystals with size up to 10 μm was observed in MCPC6. The

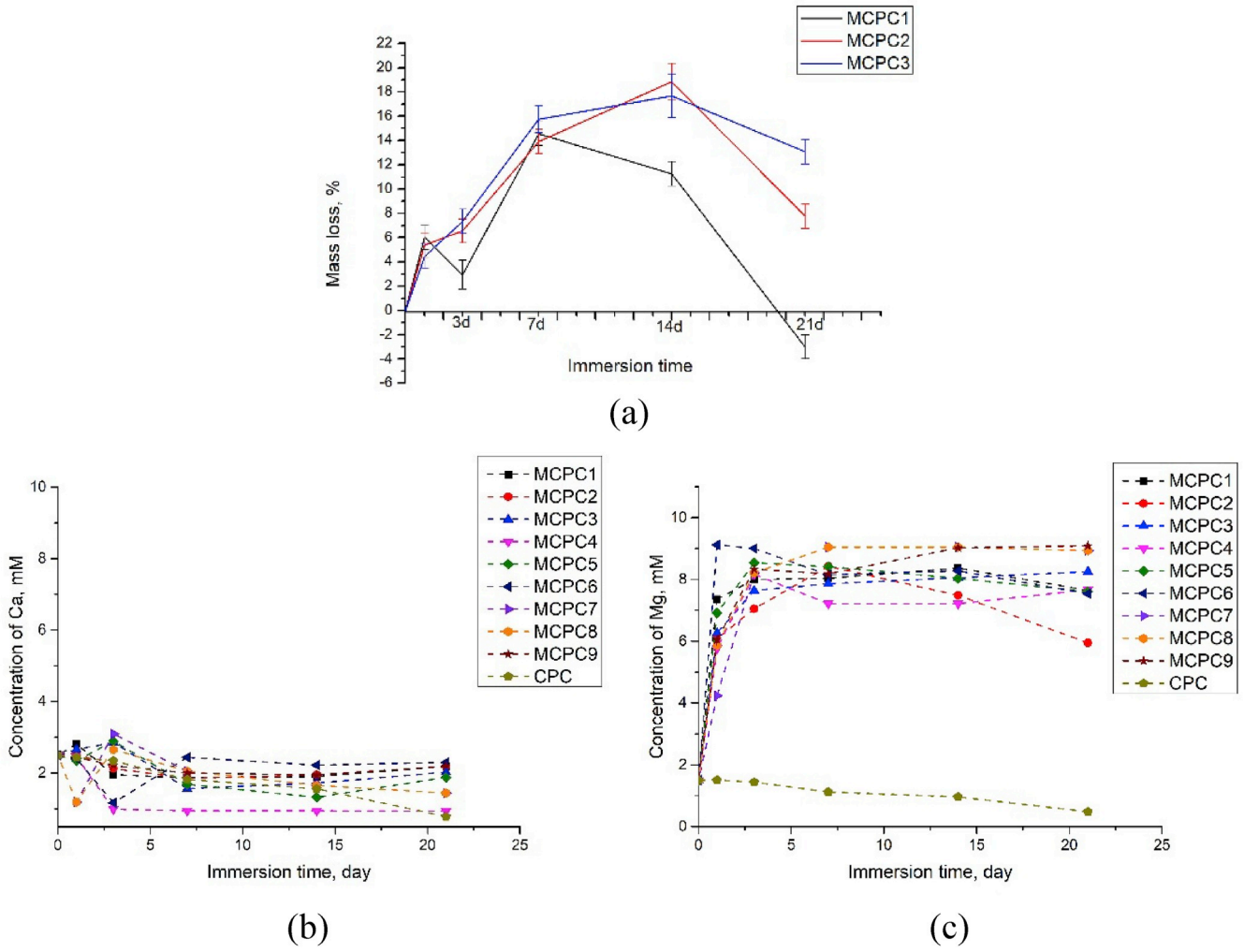

Fig. 9. The behavior of the set cements samples in the SBF solution: weight changes (a), concentrations changes of Ca^{2+} ions (b) and Mg^{2+} ions (c) in the course of the immersing.

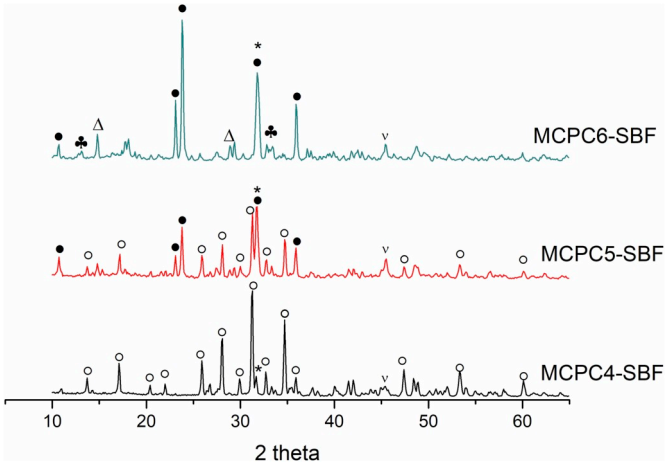

Fig. 10. XRD data of the cements samples after soaking for 21 days in SBF, where ● – stanfieldite, ○ – whitlockite ($(Ca_{2,586}Mg_{0,411})(PO_4)_2$), Δ – newberyite, ♣- $Mg_3(PO_4)*8H_2O$, * - Na_2HPO_4, ν-NaCl.

same morphology of newberyite crystals was observed during the its coating on a benchmark Ti6Al4V via microwave irradiation [32]. The further increase of (Ca + Mg)/P ratio to 2.0 resulted in a fine dense structure (Fig. 8). No recrystallization similar to cements of (Ca + Mg)/P = 1.5 and 1.67 was observed. For MCPC8 and MCPC9 (Fig. 8 c-d, e-f) numerous cracks were observed in the body of the set cement. Similar behavior had been discussed in Ref. [8] and linked with drying of the hydrated gel-like phase based on Na-contained liquid and MgO-based MPC.

For control sample (Ca/P = 2.0), CPC, the formation of loose structure with needle-like crystals of 2–5 μm in size and ~100 nm thickness on the surface of the initial powders particles was observed (Fig. 8g and h).

3.2.5. Behavior in the model liquids

In the distilled water immersion tests, the set cements initially (in 1 h) showed a slightly acidic reaction in extracts of 6.8–6.9 for the (Ca + Mg)/P = 1.5, and pH grew slightly up to ~7.2 value in 72 h (Table 4). For the compositions with (Ca + Mg)/P = 1.67, the pH values of extracts were slightly higher (7.1–7.3) after 1 h of immersion and changed insignificantly in 72 h. The (Ca + Mg)/P = 2.0 compositions demonstrated moderately high pH values of 7.8–7.9 after 1 h of immersion. pH value increased substantially with increased immersion time, reaching the values of 9.5–9.8 after 72 h for, due to interaction of preserved MgO (and probably, $MgNaPO_4*7H_2O$) with water. Similar high pH values had been previously observed in MgO-based MCP systems [8]. The evolution of extract pH in the SBF immersion tests was qualitatively similar, the values are listed in Table 3. The slightly higher values (compared to water immersion test values) observed in the case

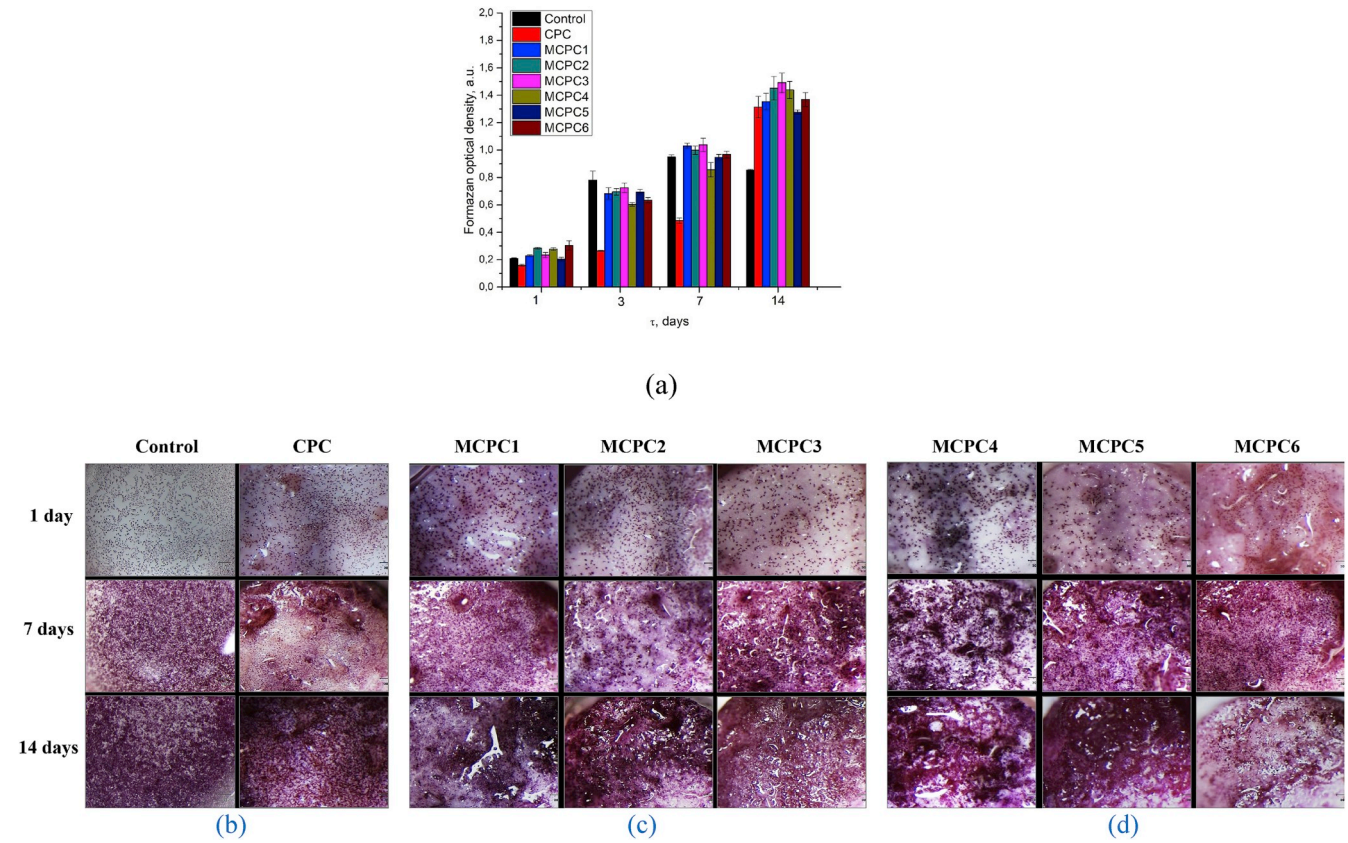

Fig. 11. The results of *in vitro* investigations of the set cements: changes of the formazan optical density for the samples at 1, 3, 7 and 14 days (a) and the view of cements samples (b – Control, CPC; c – MCPC1-3; d – MCPC4-6) in the course of investigation.

of MCPC1-6 and lower ones for MCPC7-9 were linked with presence of TRIS in the solution.

The behavior of cement samples in SBF solution was investigated via monitoring changes in the sample weight after immersion (Fig. 9 a). For all three (Ca + Mg)/P ratios, a similar trend of increased degradation rate with higher Mg content was established. It is in good agreement with [16], where tests on the mechanical mixtures of CPC and MPC showed faster degradation at high magnesium content. Expectedly, CPC cement showed the lowest degradation rate, due to presence of low-soluble HA and absence of Mg-phases. Among the three compositions, the highest degradation rate was observed for the (Ca + Mg)/P = 2.0 ratio due to the decrease of P/L ratio and significant amount of disodium phosphate. The degradation occurred due to solubility of disodium phosphate and magnesium-based phases which is confirmed by ICP revealing significantly higher concentrations of Mg compared to Ca in the extracts (Fig. 9b and c). The inversion of trend (minimum on the weight loss curve) was observed for all samples after 7–14 days of immersing (Fig. 9 a), and it was associated with recrystallization processes. It was confirmed by the decrease of Ca and Mg concentration in the 14 day extracts. According to XRD (Fig. 10), after immersing in SBF during 21 day along with the expected decrease in the intensity of the peaks of the main phases and their broadening, the newly-formed bobierrite $Mg_3(PO_4)*8H_2O$ phase was observed (most notable in the case of MCPC6). The amount of $Mg_3(PO_4)*8H_2O$ increased with growth of Mg content. The formation of NaCl crystals from the residual SBF solution after the samples drying was observed.

3.2.6. Compressive strength

Cements with (Ca + Mg)/P = 2.0 ratio are characterized by the highest values of compressive strength (Table 4). Specifically, the MCPC9 cement with a highest amount of initial MgO in cement powders demonstrated 41(3) MPa and this value is comparable with unreinforced MgO cement [6]. As it was mentioned above, this cement is characterized by a well-consolidated fine microstructure mostly based on the $MgNaPO_4*7H_2O$ crystal-hydrate with additional amorphous network [8]. The (Ca + Mg)/P = 1.67 materials are characterized by the formation of amorphous newberyite network and separate newly grown crystals. As the amount of initial MgO decreased compared to the previous series, the magnitude of strength falls down to 15–22 MPa for MCPC4-6, and maximum strength was obtained for the MCPC4 where the amount of MgO was maximal (15 wt.% according to XRD). This evidenced the primary influence of MgO amount on the mechanical properties of MCPC with NaH_2PO_4 cement liquid. The (Ca + Mg)/P = 1.5 cements with the composition based on newberyite and brushite demonstrated the lowest values of strength below 6 MPa. This fact can be interpreted using the XRD results: MCPC1-3 samples contain from 10 to 25 wt.% of brushite phase, the presence of which usually led to compressive strength decrease [33]. CPC based on TeTCP and HA is characterized by loose microstructure which resulted in a comparable low values of compressive strength.

3.2.7. In vitro investigations

According to the results of *in vitro* investigations, it can be concluded that the developed compositions of bone cements MCPC1-MCPC6 are non-toxic and have moderate matrix surface properties (Fig. 11 a). On the 10th day in the control, the formation of a confluent monolayer by cells was noted. Therefore, due to the deficiency of the culture surface, with an increase in the terms of cultivation up to 14 days, almost half of the cell pool dies (Fig. 11 b). As a result, the most representative comparison will be the number of cells after 7 days of cultivation. The best result was obtained for MCPC5 – the increase of the osteosarcoma cells population on sample compared to the control –

the polystyrene media, reaching a value of 1074 vs 0.949 a.u. For MCPC7-9 from the first day, acute cytotoxicity of the material in relation to MG-63 cells was observed. For the CPC sample, the growth of cells population was sufficiently lagging behind the control. CPC samples did not possess cytotoxicity, but the matrix surface properties were poorer compared to MCPC1-6 samples. Cytotoxicity of MCPC7-9 samples appears to be associated with high pH values of the medium (9 or more), while for MCPC1-6 samples the pH values of the medium did not exceed 7.5. It is important to note that for MCPC1-6 samples, neither the magnesium ions content nor the (Ca + Mg)/P ratio in the samples hadn't affect significantly on their matrix properties *in vitro*.

4. Conclusions

In the present paper, the powders in the magnesium calcium phosphate system with (Ca + Mg)/P ratio of 1.5 ÷ 2.0 with different Mg substitution were synthesized by one-pot process. The dominant phases are stanfieldite and whitlockite, with extra MgO phase for certain compositions. These powders were used as cement powders with NaH_2PO_4 cement liquid which warranted the absence of ammonia release opposed to commonly used $(NH_4)_2HPO_4$ liquid. In the set cements, XRD and FTIR data confirmed the formation of brushite and newberyite in the case of (Ca + Mg)/P = 1.5, newberyite in (Ca + Mg)/P = 1.67 and $NaMgPO_4$*$7H_2O$ in (Ca + Mg)/P = 2.0, respectively. The relations between phase composition, microstructure and mechanical properties of the cements, as well as setting time, pH level and behavior of the cement samples in SBF were established. The presence of MgO in initial powders resulted in a significant increase of the cement compressive strength. At the same time, in the case of (Ca + Mg)/P ratio 2.0 the high amount of MgO in initial powders which preserved after interaction with cement liquid resulted in an alkaline reaction of extracts, which probably accounts for the cytotoxicity observed in *in vitro* experiments.

In cements with (Ca + Mg)/P = 1.67 ratio MgO completely reacted with cement liquid resulting in neutral pH of extracts in distilled water and SBF immersion tests. More than threefold increase of compressive strength values was achieved compared to other cytocompatible (without MgO in initial cement powder) cements with (Ca + Mg)/P = 1.5.

Summarizing, (Ca + Mg)/P ratio 1.67 appears to be close to optimal ratio: these cements provide sufficiently high compressive strength up to 22 ± 3 MPa (for 20 mol.% of Mg) and adequate matrix properties of the surface, thus could be promising for medical applications.

Declaration of competing interest

The authors declare no conflicts of interest.

Acknowledgments

Authors are grateful for financially support by Russian Foundation for Basic Research (Grant No. 18-33-20170).

References

[1] S.M. Barinov, V.S. Komlev, Calcium phosphate bone cements, Inorg. Mater. 47 (13) (2011) 1470–1485, https://doi.org/10.1134/S002016851.
[2] M. Bohner, Design of ceramic-based cements and putties for bone graft substitution, Eur. Cell. Mater. 20 (1) (2010) 3–10, https://doi.org/10.22203/ecm.v020a01.
[3] S.M. Barinov, V.S. Komlev, Calcium Phosphate Based Bioceramics for Bone Tissue Engineering, Trans Tech Publications, Enfield, NH, USA, 2008https://doi.org/10.4028/www.scientific.net/MSFo.48.
[4] S.M. Belkoff, S. Molloy, Temperature measurement during polymerization of polymethylmethacrylate cement used for vertebroplasty, Spine 28 (14) (2003) 1555–1559, https://doi.org/10.1097/01.BRS.0000076829.54235.9F.
[5] F. Tamimi, Z. Sheikh, J. Barralet, Dicalcium phosphate cements: brushite and monetite, Acta Biomater. 8 (2) (2012) 474–487, https://doi.org/10.1016/j.actbio.2011.08.005.
[6] N. Ostrowski, A. Roy, P.N. Kumta, Magnesium phosphate cement systems for hard tissue applications: a review, ACS Biomater. Sci. Eng. 2 (7) (2016) 1067–1083, https://doi.org/10.1021/acsbiomaterials.6b00056.
[7] N. Yang, C. Shi, J. Yang, Y. Chang, Research progresses in magnesium phosphate cement–based materials, J. Mater. Civ. Eng. 26 (10) (2013) 04014071, , https://doi.org/10.1061/(ASCE)MT.1943-5533.0000971.
[8] G. Mestres, M.P. Ginebra, Novel magnesium phosphate cements with high early strength and antibacterial properties, Acta Biomater. 7 (4) (2011) 1853–1861, https://doi.org/10.1016/j.actbio.2010.12.008.
[9] G. Mestres, M. Abdolhosseini, W. Bowles, S.H. Huang, C. Aparicio, S.U. Gorr, M.P. Ginebra, Antimicrobial properties and dentin bonding strength of magnesium phosphate cements, Acta Biomater. 9 (9) (2013) 8384–8393, https://doi.org/10.1016/j.actbio.2013.05.032.
[10] C. Grobardt, A. Ewald, L.M. Grover, J.E. Barralet, U. Gbureck, Passive and active in vitro resorption of calcium and magnesium phosphate cements by osteoclastic cells, Tissue Eng. 16 (12) (2010) 3687–3695, https://doi.org/10.1089/ten.tea.2010.0281.
[11] A. Ewald, D. Kreczy, T. Brückner, U. Gbureck, M. Bengel, A. Hoess, A. Fuchs, Development and bone regeneration capacity of premixed magnesium phosphate cement pastes, Materials 12 (13) (2019) 2119, https://doi.org/10.3390/ma12132119.
[12] W. Liu, D. Zhai, Z. Huan, C. Wu, J. Chang, Novel tricalcium silicate/magnesium phosphate composite bone cement having high compressive strength, in vitro bioactivity and cytocompatibility, Acta Biomater. 21 (2015) 217–227, https://doi.org/10.1016/j.actbio.2015.04.012.
[13] T. Sopcak, L. Medvecky, M. Giretova, R. Stulajterova, J. Durisin, Hydrolysis, setting properties and in vitro characterization of wollastonite/newberyite bone cement mixtures, J. Biomater. Appl. 32 (7) (2018) 871–885, https://doi.org/10.1177/0885328217747126.
[14] G. Yang, J. Liu, F. Li, Z. Pan, X. Ni, Y. Shen, H. Xu, Q. Huang, Bioactive calcium sulfate/magnesium phosphate cement for bone substitute applications, Mater. Sci. Eng. 35 (2014) 70–76, https://doi.org/10.1016/j.msec.2013.10.016.
[15] M.A. Goldberg, V.V. Smirnov, O.S. Antonova, D.R. Khairutdinova, S.V. Smirnov, A.I. Krylov, N.S. Sergeeva, I.K. Sviridova, V.A. Kirsanova, S.A. Ahmedova, S.N. Zhevnenko, S.M. Barinov, Magnesium-substituted calcium phosphate bone cements containing MgO as a separate phase: synthesis and in vitro behavior, Mendeleev Commun. 28 (3) (2018) 329–331, https://doi.org/10.1016/j.mencom.2018.05.034.
[16] F. Wu, J. Wei, H. Guo, F. Chen, H. Hong, C. Liu, Self-setting bioactive calcium–-magnesium phosphate cement with high strength and degradability for bone regeneration, Acta Biomater. 4 (6) (2008) 1873–1884, https://doi.org/10.1016/j.actbio.2008.06.020.
[17] J. Jia, H. Zhou, J. Wei, X. Jiang, H. Hua, F. Chen, S. Wei, J.-W. Shin, C. Liu, Development of magnesium calcium phosphate biocement for bone regeneration, J. R. Soc. Interface 7 (49) (2010) 1171–1180, https://doi.org/10.1098/rsif.2009.0559.
[18] A. Ewald, K. Helmschrott, G. Knebl, N. Mehrban, L.M. Grover, U. Gbureck, Effect of cold- setting calcium- and magnesium phosphate matrices on protein expression in osteoblastic cells, J. Biomed. Mater. Res. B Appl. Biomater. 96 (2) (2011) 326–332, https://doi.org/10.1002/jbm.b.31771.
[19] W.L. Hill, G.T. Faust, D.S. Reynolds, The binary system P_2O_5 ; 2CaO; P_2O_5, AJS Online September 242 (9) (1944) 457–477 https://doi/10.2475/ajs.242.9.457.
[20] E.V. Shelekhov, T.A. Sviridova, Programs for X-ray analysis of polycrystals, Met. Sci. Heat Treat. 42 (8) (2000) 309–313, https://doi.org/10.1007/BF02471306.
[21] Tadashi Kokubo, Surface chemistry of bioactive glass-ceramics, J. Non-Cryst. Solids 120 (1–3) (1990) 138–151, https://doi.org/10.1016/0022-3093(90)90199-V.
[22] Tim Mosmann, Rapid colorimetric assay for cellular growth and survival: application to proliferation and cytotoxicity assays, J. Immunol. Methods 65 (1–2) (1983) 55–63, https://doi.org/10.1016/0022-1759(83)90303-4.
[23] R.A. Terpstra, F.C.M. Driessens, R.M.H. Verbeeck, The CaO- MgO- P_2O_5 system at 1000° C for P_2O_5 33.3 mole%, Z. Anorg. Allg. Chem. 515 (8) (1984) 213–224, https://doi.org/10.1002/zaac.19845150825.
[24] J.V. Rau, V. M Wu, V. Graziani, I.V. Fadeeva, A.S. Fomin, M. Fosca, V. Uskoković, The bone building blues: self-hardening copper-doped calcium phosphate cement and its in vitro assessment against mammalian cells and bacteria, Mat. Sci. Eng. C. Mater. 79 (2017) 270–279, https://doi.org/10.1016/j.msec.2017.05.052.
[25] S. Raynaud, E. Champion, D. Bernache-Assollant, P. Thomas, Calcium phosphate apatites with variable Ca/P atomic ratio I. Synthesis, characterisation and thermal stability of powders, Biomaterials 23 (4) (2002) 1065–1072, https://doi.org/10.1016/S0142-9612(01)00218-6.
[26] N.I. Khan, K. Ijaz, M. Zahid, A.S. Khan, M.R.A. Kadir, R. Hussain, A.A. Chaudhry, Microwave assisted synthesis and characterization of magnesium substituted calcium phosphate bioceramics, Mater. Sci. Eng. 56 (2015) 286–293, https://doi.org/10.1016/j.msec.2015.05.025.
[27] A. Ansari, A. Ali, M. Asif, Microwave-assisted MgO NP catalyzed one-pot multicomponent synthesis of polysubstituted steroidal pyridines, New J. Chem. 42 (1) (2018) 184–197 http://xlink.rsc.org/?DOI=c7nj03742b.
[28] Z. Qin, C. Ma, Z. Zheng, G. Long, B. Chen, Effects of metakaolin on properties and microstructure of magnesium phosphate cement, Construct. Build. Mater. 234 (2020) 117353, https://doi.org/10.1016/j.conbuildmat.2019.117353.
[29] L. Qin, W. Zhang, J. Lu, A.G. Stack, L. Wang, Direct imaging of nanoscale dissolution of dicalcium phosphate dihydrate by an organic ligand: concentration matters, Environ. Sci. Technol. 47 (23) (2013) 13365–13374, https://doi.org/10.1021/es402748t.
[30] M. Mathew, P. Kingsbury, S. Takagi, W.E. Brown, A new struvite-type compound, magnesium sodium phosphate heptahydrate, Acta Crystallogr. Sect. B Struct.

Crystallogr. Cryst. Chem. 38 (1) (1982) 40–44, https://doi.org/10.1107/S0567740882002003.
[31] P.F. Franczak, N.H.A. Camargo, N. Levandowski, D.F. da Silva, Synthesis and characterization of three hydrated calcium phosphates used as biocement precursors, Adv. Mater. Res. 936 (2014) 712–716 https://doi.org/10.4028/www.scientific.net/AMR.936.712.
[32] P. Sikder, C.R. Grice, S.B. Bhaduri, Processing-structure-property correlations of crystalline antibacterial magnesium phosphate (newberyite) coatings and their in vitro effect, Surf. Coating. Technol. 374 (2019) 276–290, https://doi.org/10.1016/j.surfcoat.2019.06.007.
[33] J. Engstrand, C. Persson, H. Engqvist, The effect of composition on mechanical properties of brushite cements, J. Mech. Behav.Biomed. Mater. 29 (2014) 81–90, https://doi.org/10.1016/j.jmbbm.2013.08.024.